

RSC Advances



This is an *Accepted Manuscript*, which has been through the Royal Society of Chemistry peer review process and has been accepted for publication.

Accepted Manuscripts are published online shortly after acceptance, before technical editing, formatting and proof reading. Using this free service, authors can make their results available to the community, in citable form, before we publish the edited article. This *Accepted Manuscript* will be replaced by the edited, formatted and paginated article as soon as this is available.

You can find more information about *Accepted Manuscripts* in the [Information for Authors](#).

Please note that technical editing may introduce minor changes to the text and/or graphics, which may alter content. The journal's standard [Terms & Conditions](#) and the [Ethical guidelines](#) still apply. In no event shall the Royal Society of Chemistry be held responsible for any errors or omissions in this *Accepted Manuscript* or any consequences arising from the use of any information it contains.

1 **One-Pot Synthesis of 3D flower-like heterostructured SnS₂/MoS₂ for enhanced**
2 **Supercapacitor Behaviors**

3

4 *Lina Wang^{a,b}, Ying Ma^{a,b}, Min Yang^a, Yanxing Qi^{a,*}*

5 a.State Key Laboratory for Oxo Synthesis and Selectve Oxidation, Lanzhou Institute of Chemical

6 Physics, Chinese Academy of Sciences, Lanzhou 730000, PR China.

7 b.University of Chinese Academy of Sciences, Beijing 100039, PR China.

8 Corresponding author. Tel./fax: +86 931 4968190.

9 E-mail addresses: wanglina1106@126.com, qiya@lzb.ac.cn(Y.Qi).

10 **Abstract:** Novel three-dimensional flower-like heterostructured SnS₂/MoS₂ was produced via one-step
11 hydrothermal method. The full potential of the heterostructured SnS₂/MoS₂ material could be realized
12 because of strong synergetic effect, which was not only able to effectively weaken the agglomerating
13 and restacking problems during the electrochemical reaction, but also able to ensure the high-rate and
14 long-life. We found that the SnS₂/MoS₂ had better electrochemical performance compared to the MoS₂,
15 due to the rapid electronic transport and volume change buffering of the formation of SnS₂/MoS₂
16 heterostructure. The electrochemical tests showed that the SnS₂/MoS₂ electrode had a specific
17 capacitance of 105.7 F g⁻¹ at a current density of 2.35 A g⁻¹ and it displayed good cyclic stability of
18 90.4% retention even after 1000 cycles, which indicated that the SnS₂/MoS₂ was an useful potential
19 electrode material for the application of energy storage and deserved to be further investigated.

20 **Keywords:** molybdenum disulfide, tin disulfide, heterostructured nanomaterial, energy storage,
21 supercapacitor

22 **1. Introduction**

23 To meet the urgent needs for renewable and sustainable power sources, great attention has been
24 focused on storage devices and energy conversion with ultra fast charge and discharge characteristics,

1 such as supercapacitors ^[1-3]. Supercapacitors are a new energy storage with high power density, fast
2 charging/discharging rate, super-long cycle life, and excellent cycle stability^[4-7].

3 Three-dimensional (3D) hierarchical structures, which are comprised of low dimensional nanosheets
4 building blocks nanostructures, are promising as electrodes ^[8-11]. Because 3D hierarchical structures
5 exhibit the advantages of the pristine building blocks and the improvement property of their secondary
6 architecture. With regard to Supercapacitor, the 3D hierarchical structures can facilitate the
7 transportation of electrons and ions and accommodate the volume change of materials in
8 electrochemical reaction process ^[12-14].

9 Molybdenum disulfide (MoS₂), as an important member of two-dimensional(2D) nanomaterials, is
10 composed of three atom layers (S-Mo-S) stacking together via weak van der Waals interaction. Up to
11 now, 3D hierarchical structures MoS₂, such as flower-like nanostructures ^[15], hierarchically porous
12 hollow spheres ^[16-18], have been proved to be effective in improving their electrochemical properties. In
13 general, self-assembled style, which minimize the energy of the reactive system in a spontaneous
14 process, is the simplest synthetic route to obtain 3D hierarchical structures^[19]. However, the design and
15 electric reactivity of 3D nano-heterostructures have rarely been studied. Kim et al. reported the MoS₂
16 nanostructures synthesized by a hydrothermal route and the specific capacitance of MoS₂ was 92.85
17 Fg⁻¹ at a constant discharge current density of 0.5 mA cm⁻²^[20]. Ma and co-workers synthesized
18 flower-like MoS₂ nanospheres through a hydrothermal method. However, the electrochemical tests
19 showed that the maximum specific capacity was just about 122 F g⁻¹ at 1 A g⁻¹^[21]. Sun et al
20 demonstrated polyaniline/MoS₂ composites for high-performance supercapacitors and the specific
21 capacitance of the pure MoS₂ electrodes was only 98 F g⁻¹ at 1 A g⁻¹^[22]. However, the rate
22 performances and cycling stabilities of the electrode materials are still unsatisfactory. Ternary sulfides,

1 such as nickel-cobalt sulfides, exhibit an electric conductivity that is much higher than those of single
2 component sulfides. For example, Chen et al reported that the hierarchical structured $\text{Ni}_x\text{Co}_{1-x}\text{S}_{1.097}$
3 electrodes exhibited a remarkable maximum specific capacitance of approximately five times higher
4 than that of the $\text{CoS}_{1.097}$ precursors at a current density of 0.5 A g^{-1} ^[23]. Chen and colleagues proved that
5 the specific capacitance of $\text{Ni@Ni}_3\text{S}_2$ was improved from 89 F g^{-1} to 122 F g^{-1} for $\text{Ni@Ni}_{1.4}\text{Co}_{1.6}\text{S}_2$ at a
6 current density of 1 A g^{-1} with a high loading level (20 mg cm^{-2}). The as-assembled
7 $\text{Ni@Ni}_{1.4}\text{Co}_{1.6}\text{S}_2//\text{AC}$ showed better cycling stability and coulombic efficiency than $\text{Ni@Ni}_3\text{S}_2//\text{AC}$ ^[24].
8 Guan and colleagues fabricated a 3D hierarchical nest-like $\text{Ni}_3\text{S}_2@\text{NiS}$ with nanorods as building
9 blocks, which was then used as template to prepare $\text{Ni}_3\text{S}_2@\text{Co}_9\text{S}_8$ and NiS@NiSe_2 electrodes. The
10 specific capacities of $\text{Ni}_3\text{S}_2@\text{NiS}$, $\text{Ni}_3\text{S}_2@\text{Co}_9\text{S}_8$, and NiS@NiSe_2 electrodes were 2440, 6427, and 7717
11 F g^{-1} , respectively, at a current density of 0.5 A g^{-1} ^[25]. The results indicated that the synergistic effect of
12 double metal ions could enhance the electrochemical performance .

13 Herein, we report the preparation of MoS_2 3D hierarchical structures with grown SnS_2 by a
14 simple one-pot approach without using any toxic chemicals. In this nanostructure, Sn ions can be
15 readily embedded onto the flowerlike MoS_2 nanosheets through one-top hydrothermal technique.
16 And three-dimensional flowerlike heterostructured $\text{SnS}_2/\text{MoS}_2$ nanosheets act as framework-like
17 substrate to provide a path for ions diffusion. In the nanostructure, SnS_2 nanoplates reside in the
18 flowerlike MoS_2 nanosheets to prevent the collapse of the MoS_2 nanosheets. Thereby, the
19 synergistic effect of MoS_2 nanosheets and SnS_2 nanoplates is not only able to effectively weaken
20 the agglomerating and restacking problems during the electrochemical reaction, but also able to
21 ensure the high-rate and long-life. The structure, morphology and electrochemical performance of
22 the electrode material were investigated. The as-prepared $\text{SnS}_2/\text{MoS}_2$ electrode exhibits a high

1 capacitance of 105.4F g^{-1} at 2.35A g^{-1} , and also shows excellent cycle stability. The results
2 confirm that the as-prepared heterostructured $\text{SnS}_2/\text{MoS}_2$ nanostructured electrode exhibits an
3 enhanced electrochemical behavior.

4 **2. Experimental section**

5 **2.1 Materials**

6 Sodium molybdate, thiourea, and tin tetrachloride were of analytical grade and used without
7 further purification. In a typical procedure, $2.4\text{mm Na}_2\text{MoO}_4 \cdot 2\text{H}_2\text{O}$, 0.8mm SnCl_4 and 9mm
8 $(\text{NH}_2)_2\text{CS}$ were dissolved in 15 ml of deionized water and 5ml of absolute ethanol. After stirring
9 for 30 min , the solution was transferred into a 50 ml Teflon-lined stainless steel autoclave and
10 sealed tightly and then heated at $210\text{ }^\circ\text{C}$ for 22 h . After cooling naturally, the black precipitates
11 were collected, washed by deionized water several times, and dried at $80\text{ }^\circ\text{C}$ for 5 h in a vacuum
12 oven. Finally, the hierarchical heterostructured $\text{SnS}_2/\text{MoS}_2$ were obtained. As a comparison, 3D
13 flower-like MoS_2 was obtained, when $2.4\text{mm Na}_2\text{MoO}_4 \cdot 2\text{H}_2\text{O}$ and $4.8\text{mm}(\text{NH}_2)_2\text{CS}$ were dissolved in
14 15 ml of deionized water and 5ml of absolute ethanol with the other reaction conditions left unchanged.

15 **2.2 Characterization**

16 The crystal structure of the obtained $\text{SnS}_2/\text{MoS}_2$ was characterized by X-ray diffraction (XRD) on a
17 PANalytical X'pert PRO instrument using $\text{Cu K}\alpha$ radiation. The morphology of the sample was
18 studied by transmission electron microscope (TEM) on a JEOLJEM-2100 instrument at an accelerating
19 voltage of 80 kV and field-emission scanning electron microscope (FESEM) using a JEOL-JSM6701F
20 instrument at an accelerating voltage of 5 kV . The qualitative information was obtained by X-ray
21 Photoelectron Spectrometer (XPS, VG ESCALAB 210)

22 **2.3 Electrochemical Measurements**

23 A typical three electrode test cell was used for capacitive performances of the as-prepared sample

1 on a CHI660D (Chenhua, Shanghai, China) electrochemical working station. All of the measurements
2 were carried out in a 1 M KCl aqueous electrolyte solution at room temperature. The working electrode
3 was fabricated by mixing the as-prepared electroactive material, carbon black and poly(tetra
4 fluoroethylene) at a weight ratio of 85:10:5 to form a homogeneous slurry (the total mass of the
5 electrode material was 10 mg), which was pasted onto a piece of nickel foam current collector using a
6 blade. Afterwards, the electrode was dried at 80°C for 12h. A saturated calomel electrode (SCE) and
7 platinum sheet were used as the reference and counter electrodes, respectively. Cyclic voltammetry
8 (CV) measurements were carried out in the potential range from -0.9 V to -0.3 V using different scan
9 rates, which was varied from 2 to 20 mV s⁻¹. Galvanostatic charge-discharge (GCD) curves were
10 recorded at different current densities within the potential range from -0.9 V to -0.3 V. Electrochemical
11 impedance spectroscopy (EIS) measurements were performed in the frequency range of 10⁵ to 10⁻² Hz.

12 **3. Results and Discussion**

13 The XRD pattern of the SnS₂/MoS₂ displays two kinds of diffraction peaks in figure 1, Besides the
14 diffraction peaks at 13.9° (002), 33.3° (100) and 57.5° (006) reflections assigned to the MoS₂
15 (JCPDS card no.37-1492)^[26], all additional ones are well-matched to the SnS₂ (JCPDS #23-0677)^[27]
16 indicating the presence of SnS₂ grown with MoS₂.

17 The low-magnification SEM image (Fig. 2a) demonstrates that the MoS₂ consists of a large quantity
18 of uniform 3D flower-like nanostructures. The flower-like MoS₂ has diameters of about 600-800 nm.
19 The high-magnification SEM image (Fig. 2b) reveals that the flower-like nanostructures are composed
20 of intercrossed curved nanoflakes with a thickness of several nanometers. The morphology of the
21 as-synthesized flowerlike MoS₂ was further characterized by TEM. As shown in Fig. 2c, TEM image
22 confirms the existence of flowerlike MoS₂ structures, which closely correlates with the results of the
23 SEM measurement. Figure 3(a,b) shows the SEM image of the as prepared flower-like SnS₂ /MoS₂

1 heterostructure. The 3D architecture is helpful to increase the specific area. 3D flower-like
2 heterostructured MoS₂/SnS₂ facilitates rapid electronic transport in electrode reactions. Furthermore,
3 this structure also enhances the stability of electrochemical performance. Figure 3c shows the TEM
4 image of SnS₂/MoS₂ heterostructure. The image reveals a general trend with the sheets of SnS₂
5 homogeneously embedded in MoS₂, showing the layered platelets. The Mapping analyses on the
6 SnS₂/MoS₂ (Figure 3d) reveal the presence of not only Mo and S but also Sn, which confirm the
7 assumption that some SnS₂ may be formed in the interior of MoS₂. Inductively coupled plasma mass
8 spectroscopy analysis reveals that the ratio of Mo:Sn was 3.4:1.

9 The obtained SnS₂/MoS₂ were further characterized by XPS. The high-resolution XPS of Mo 3d
10 exhibits three peaks in Fig. 4a. The peaks at 233.1 and 229.9 eV are Mo 3d_{3/2} and Mo 3d_{5/2} binding
11 energies, respectively. These peaks can be attributed to the Mo ion in the +4 oxidation state. The peak
12 at 227.1 eV can be ascribed to the 2s binding energy of S in MoS₂. The high-resolution of S 2p spectrum
13 showed main doublet located at binding energies of 162.1 and 163.2 eV in Fig. 4b, which can be
14 assigned to the spin-orbit couple S 2p_{3/2} and S 2p_{1/2}, respectively. These binding energies agree
15 well with the reported values for the MoS₂ [28-29]. The two strong peaks at around 486.5 and 495
16 eV are displayed in Fig. 3c. These peaks can be attributed to Sn 3d_{3/2} and 3d_{5/2} respectively, which
17 are consistent with the reference data of Sn⁴⁺ in SnS₂ [30].

18 The electrochemical measurement results of the MoS₂ and SnS₂/MoS₂ electrodes were evaluated by
19 cyclic voltammetry (CV). Fig. 5a shows the cyclic voltammograms curves of the SnS₂/MoS₂ electrode
20 at various scan rates ranging from 2 to 20 mV s⁻¹ in a potential range of -0.9 V to -0.3 V. It can be
21 observed that all the curves exhibit an approximately rectangular shape without any redox peaks which
22 indicates a typical electrical double-layer capacitance feature with fast charging-discharging processes.

1 In addition, the shapes of these CV curves do not significantly change with increasing scan rate from 2
2 to 20 mV s⁻¹, which reveals the ideal capacitive behavior and good charge collection as well as the
3 facilitated diffusion of K⁺ in the SnS₂/MoS₂ electrode^[31]. Furthermore, the CV curve area increases
4 with the scan rate, indicating that the rates of electric and proton transportation are rapid with respect to
5 the scan rates. The normalized CV of MoS₂ nanoflowers at the scan rate of 10 mV S⁻¹ have also been
6 measured and shown for comparison with SnS₂/MoS₂ in Figure 5b. Obviously, the SnS₂/MoS₂ owns
7 larger enclosed area than pure MoS₂, suggesting that the former has a larger areal capacitance. This is
8 mainly due to the great contribution of the SnS₂/MoS₂, which prevents the collapse of the MoS₂
9 nanosheets. Thereby, the synergistic effect of MoS₂ nanosheets and SnS₂ nanoplates is not only
10 able to effectively weaken the agglomerating and restacking problems, but also able to facilitate
11 rapid electronic transport in electrode reactions.

12 To further calculate the specific capacitance of the 3D flower-like heterostructured SnS₂/MoS₂
13 electrode, the charge/discharge measurements were performed between -0.9 V to -0.3 V at different
14 current densities in 1 M KCl solutions as shown in Fig. 3c. The specific capacitance was calculated by
15 the following equation:

$$16 \quad C_m = \frac{It}{m\Delta V}$$

17 where C_m (F g⁻¹) is the specific capacitance, I (A) is the discharge current, t (s) is the discharge time,
18 ΔV (V) is the potential window, and m (g) is the mass of the active material.

19 According to the equation, the specific capacitances of the SnS₂/MoS₂ are 151.9, 127.4, 111.3, and
20 105.7 F g⁻¹ at 0.24, 0.59, 1.18, and 2.35 A g⁻¹, respectively (Figure 5c). At low current densities, the
21 inner active sites or the pores of the electrode can be fully accessed and diffused with cations; hence,
22 high specific capacitance values are achieved. The charge/discharge behavior of MoS₂ had also been

1 measured and showed in Figure 5d. The capacitance of the electrode is calculated to be about 145.8,
2 125.1, 100.3 and 67.3 F g⁻¹ at 0.24, 0.59, 1.18, and 2.35 A g⁻¹, respectively. They own low capacitance
3 (67.3 F g⁻¹ at 2.35 A g⁻¹) compared to SnS₂/MoS₂ electrode, which deliver an improved capacitance.
4 The enlarged specific capacitance can be attributed to the synergistic effect of two-component
5 heterostructured metal sulfides.

6 Fig. 6a shows Nyquist plots of the EIS data obtained for the SnS₂/MoS₂ and MoS₂ electrodes at open
7 circuit potential over the frequency range 0.01-100,000 Hz in 1M KCl electrolyte solutions. In low
8 frequency area, the Warburg impedance (W), which results from the diffusive resistance of the
9 electrolyte into the interior of the electrode and the ion diffusion into the electrode, is shown by the
10 slope of the curve. The more vertical the curve is, the smaller Warburg impedance is. The slopes of the
11 curve at low frequency area of SnS₂/MoS₂ electrode is more vertical compared to MoS₂, which
12 demonstrates the decreasing of diffusive resistance between the electrode and the electrolyte. In the
13 high frequency area, the semicircle corresponds to the charge-transfer resistance of the electrode and
14 electrolyte interface^[32-33]. Different from pure MoS₂, the semicircle is smaller in SnS₂/MoS₂ electrode,
15 indicating that the resistance is significant lower. The bulk resistance of the electrochemical system can
16 also be realized from the intersection of the curve at real part Z. From the plots, we can see SnS₂/MoS₂
17 electrode shows lower bulk resistance.

18 The cycling stability of the SnS₂/MoS₂ electrode was investigated by repeating the galvanostatic
19 charge-discharge measurements ranging from -0.9V to -0.3 V over 1000 cycles at the current density of
20 2.35A g⁻¹, as shown in Figure 6b. The specific capacitance gradually decreases with the cycle number,
21 and the specific capacitance of this electrode still remains at 90.4% after 1000 cycles. Figure 4b also
22 shows the cycle characteristic of pure MoS₂ at a current density of 2.35 A g⁻¹ for up to 500 cycles. After

1 that, it only retains 79% of the initial capacitance with a quite quick decrease. It is clear that the cycle
2 stability of SnS₂/MoS₂ are greatly improved. The excellent electrochemical performance can be
3 attributed to SnS₂/MoS₂ heterostructure, which forms an interconnected conducting network, and
4 facilitates rapid electronic transport in electrode reactions.

5 **4. Conclusions**

6 In summary, we have demonstrated a one-step hydrothermal way to fabricate 3D flower-like
7 heterostructured SnS₂/MoS₂, which had better electrochemical performance compared to the MoS₂.
8 The as-prepared SnS₂/MoS₂ electrode exhibited a high capacitance of 105.4F g⁻¹ at 2.35A g⁻¹, and also
9 showed excellent cycle stability. This capacitive behavior mainly resulted from the the rapid electronic
10 transport and volume change buffering of SnS₂/MoS₂ heterostructure during electrochemical
11 measurement. Due to the excellent performance, we believe that the SnS₂/MoS₂ is a potential
12 promising electrode material for the application of energy storage or conversion with fine
13 electrochemical performance and deserved to be further investigated.

14 **Author Information**

15

16 **Corresponding Author**

17 *E-mail: wanglina1106@126.com, qiya@lzb.ac.cn.

18 **Notes**

19 The authors declare no competing financial interest.

20 **Acknowledgments**

21 This work is supported by the Chinese Academy of Sciences and Technology Project (XBLZ-2011-013)
22 and the Technologies R&D Program of Gansu Province (1104FKCA156).

23 **References**

- 24 [1] Winter, M.; Brodd, R. J. What Are Batteries, Fuel Cells, and Supercapacitors. Chem. Rev. 2004, 10,
25 4245-4270.
- 26 [2] Zhu, Y.; Murali, S.; Stoller, M. D.; Ganesh, K. J.; Cai, W.; Ferreira, P. J.; Pirkle, A.; Wallace, R. M.;

- 1 Cychosz, K. A.; Thommes, M.; Su, D.; Stach, E. A.; Ruoff, R. S. Carbon-Based Supercapacitors
2 Produced by Activation of Graphene. *Science* 2011, 332, 1537-1541.
- 3 [3] Tarascon, J. M. Armand, M. Issues and Challenges Facing Rechargeable Lithium Batteries. *Nature*
4 2001, 414, 359-367.
- 5 [4] Conway, B. E.; Birss, V. ; Wojtowicz, J. The Role and Utilization of Pseudocapitance for
6 Energy Storage by Supercapacitors. *J. Power Sources* 1997, 66, 1-14.
- 7 [5] Pech, D.; Brunet, M.; Durou, H.; Huang, P.; Mochalin, V.; Gogotsi, Y.; Taberna, P. L.; Simon, P.
8 Ultrahigh-power Micrometre-sized Supercapacitors Based on Onion-like Carbon. *Nat. Nanotech.* 2010,
9 5, 651-654.
- 10 [6] Mahmood, N.; Zhang, C.; Yin, H.; Hou, Y. Graphene-based Nanocomposites for Energy storage and
11 Conversion in Lithium Batteries, Supercapacitors and Fuel cells. *J. Mater. Chem. A* 2014, 2, 15-32.
- 12 [7] Simon, P.; Gogotsi, Y.; Dunn, B. Where Do Batteries End and Supercapacitors Begin. *Science* 2014,
13 343, 1210-1211.
- 14 [8] Li, B.; Wang, Y. Facile Synthesis and Enhanced Photocatalytic Performance of Flower-like ZnO
15 Hierarchical Microstructures. *J Phys Chem C* 2009, 114, 890-896.
- 16 [9] Tiwari, J.N.; Tiwari, R.N.; Kim, K.S. Zero-dimensional, One-dimensional, Two-dimensional and
17 Three-dimensional Nanostructured Materials for Advanced Electrochemical Energy Devices. *Prog*
18 *Mater Sci* 2012, 57, 724-803.
- 19 [10] Hu, C.; Guo, J.; Wen, J. Hierarchical Nanostructure CuO with Peach Kernel-like Morphology as
20 Anode Material for Lithium-ion Batteries. *Ionics* 2013, 19, 253-258.
- 21 [11] Zhu, J.; Yin, Z.; Yang, D.; Sun, T.; Yu, H.; Hoster, H. E.; Hng, H.H.; Zhang, H.; Yan, Q.
22 Hierarchical Hollow Spheres Composed of Ultrathin Fe₂O₃ Nanosheets for Lithium Storage and

- 1 Photocatalytic Water Oxidation. *Energy Environ Sci* 2013, 6, 987-993.
- 2 [12] Wang, J.; Du, G.; Zeng, R.; Niu, B.; Chen, Z.; Guo, Z.; Dou, S. Porous Co_3O_4 Nanoplatelets by
3 Self-supported Formation as Electrode Material for Lithium-ion Batteries. *Electrochim Acta* 2010, 55,
4 4805-4811.
- 5 [13] Park, M. H.; Kim, K.; Kim, J.; Cho, J. Flexible Dimensional Control of High-Capacity
6 Li-Ion-Battery Anodes: From 0D Hollow to 3D Porous Germanium Nanoparticle Assemblies. *Adv*
7 *Mater* 2010, 22, 415-418.
- 8 [14] Esmanski, A.; Ozin, G. A. Silicon Inverse-Opal-Based Macroporous Materials as Negative
9 Electrodes for Lithium Ion Batteries. *Adv Funct Mater* 2009, 19, 1999-2010.
- 10 [15] Huang, K. J.; Wang, L.; Liu, Y. J.; Wang, H. B.; Liu, Y. M.; Wang, L. L. Synthesis of
11 polyaniline/2-dimensional graphene analog MoS_2 composites for high-performance supercapacitor.
12 *Electrochim. Acta* 2013, 109, 587-594.
- 13 [16] Wan, Z. M.; Shao, J.; Yun, J. J.; Zheng, H. Y.; Gao, T.; Shen, M.; Qu, Q. T.; Zheng, H. H.
14 Core-Shell Structure of Hierarchical Quasi-Hollow MoS_2 Microspheres Encapsulated Porous Carbon
15 as Stable Anode for Li-Ion Batteries. *Small* 2014, 10, 4975-4981.
- 16 [17] Dhas, N. A.; Suslick, K. S. Sonochemical Preparation of Hollow Nanospheres and Hollow
17 Nanocrystals. *J. am. chem. soc.* 2005, 127, 2368-2369.
- 18 [18] Wang, M.; Li, G. D.; Xu, H. Y.; Qian, Y. T.; Yang, J. Enhanced Lithium Storage Performances of
19 Hierarchical Hollow MoS_2 Nanoparticles Assembled from Nanosheets. *ACS Appl. Mater. Interfaces*
20 2013, 5, 1003-1008.
- 21 [19] Ma, J.; Lei, D.; Duan, X.; Li, Q.; Wang, T.; Cao, A.; Mao, Y.; Zheng, W. Designable Fabrication of
22 Flower-like SnS_2 Aggregates with Excellent Performance in Lithium-ion Batteries. *RSC Adv* 2012, 2,

- 1 3615-3617.
- 2 [20] Krishnamoorthy, K.; Veerasubramani, G. K.; Radhakrishnan, S.; Kim, S. J. Supercapacitive
3 properties of hydrothermally synthesized sphere like MoS₂ nanostructures. Mater. Res. Bull. 2014,
4 50,499-502.
- 5 [21] Zhou, X.; Xu, B.; Lin, Z.; Shu, D.; Ma, L. Hydrothermal Synthesis of Flower-Like MoS₂
6 nanospheres for Electrochemical Supercapacitors. J. Nanosci. Nanotechnol. 2014, 14, 7250-7254.
- 7 [22] Hu, B.; Qin, X.; Asiri, A. M.; Alamry, K. A.; AlYoubi, A. O.; Sun, X. Synthesis of porous
8 tubular C/MoS₂ nanocomposites and their application as a novel electrode material for
9 supercapacitors with excellent cycling stability. Electrochim. Acta 2013, 100,24-28.
- 10 [23] Gao, Y.; Cui, S.; Mi, L.; Wei, W.; Yang, F.; Zheng, Z.; Hou, H.; Chen, W. Double Metal Ions
11 Synergistic Effect in Hierarchical Metal Sulfide Microflowers for Enhanced Supercapacitor
12 Performance. ACS Appl. Mater. Interfaces, 2015, 7, 4311-4319.
- 13 [24] Mi, L.; Wei, W.; Huang, S.; Cui, S.; Zhang, W.; Hou, H.; Chen, W. Nest-like Ni@Ni_{1.4}Co_{1.6}S₂
14 Electrode for Flexible High-Performance Rolling Supercapacitors Device Design. J. Mater. Chem.
15 A, 2015, DOI: 10.1039/C5TA06265A.
- 16 [25] Wei, W.; Mi, L.; Gao, Y.; Zheng, Z.; Chen, W.; Guan, X. Partial Ion-Exchange of
17 Nickel-Sulfide-Derived Electrodes for High Performance Supercapacitors. Chem. Mater. 2014, 26,
18 3418-3426.
- 19 [26] Luo, H.; Xu, C.; Zou, D.; Wang, L.; Ying, T. Hydrothermal synthesis of hollow MoS₂ micro-
20 spheres in ionic liquids/water binary emulsions. Mater. Lett. 2008, 62, 3558-3560.
- 21 [27] Jana, M. K.; Rajendra, H. B.; Bhattacharyya, A. J.; Biswas, K. Green ionothermal synthesis of
22 hierarchical nanostructures of SnS₂ and their Li-ion storage properties. CrystEngComm 2014,16,

- 1 3994-4000.
- 2 [28] Li, W. J.; Shi, E. W.; Ko, J. M.; Chen, Z.; Ogino, H.; Fukuda, T. J. Hydrothermal synthesis of
- 3 MoS₂ nanowires. *Crystal Growth & Design*. 2003, 250,418-422.
- 4 [29] Lin, H.; Chen, X.; Li, H.; Yang, M.; Qi, Y. Hydrothermal synthesis and characterization of MoS₂
- 5 nanorods. *Mater. Lett.* 2010, 64, 1748-1750.
- 6 [30] Zhang, Y.; Li, J.; Zhang, M.; Dionysiou, D. D. Size-tunable hydrothermal synthesis of SnS₂
- 7 nanocrystals with high performance in visible light-driven photocatalytic reduction of aqueous Cr(VI).
- 8 *Environ. Sci. Technol.* 2011, 45, 9324-9331.
- 9 [31] Li, J.; Yang, Q.M.; Zhitomirsky, I. Nickel foam-based manganese dioxide-carbon nanotube
- 10 composite electrodes for electrochemical supercapacitors. *J. Power Sources* 2008, 185, 1569-1574.
- 11 [32] Oswald, H. R.; Gunter, J. R.; Dubler, E. J. Topotactic decomposition and crystal structure of white
- 12 molybdenum trioxide-monohydrate: Prediction of structure by topotaxy. *Solid State Chem.* 1975, 13,
- 13 330-338.
- 14 [33]Nagasawa, T.; Kobayashi, K. Paracrystalline Structure of Polymer-Crystal Lattice Distortion
- 15 Induced by Electron Irradiation. *J. Appl. Phys.* 1970, 41, 4276-4284.

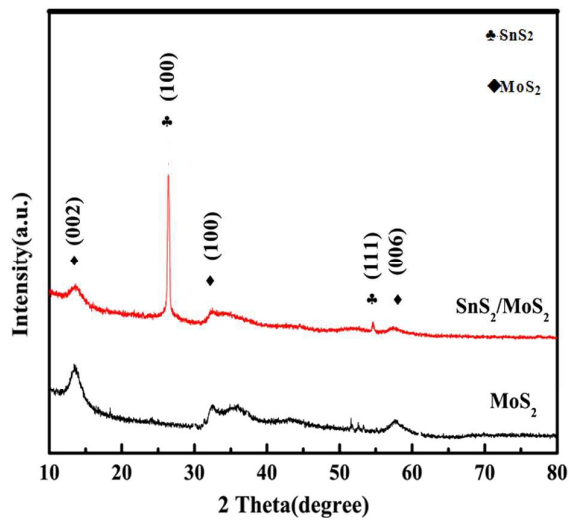


Figure 1. XRD patterns of the flower-like MoS₂ and heterostructured SnS₂/MoS₂.

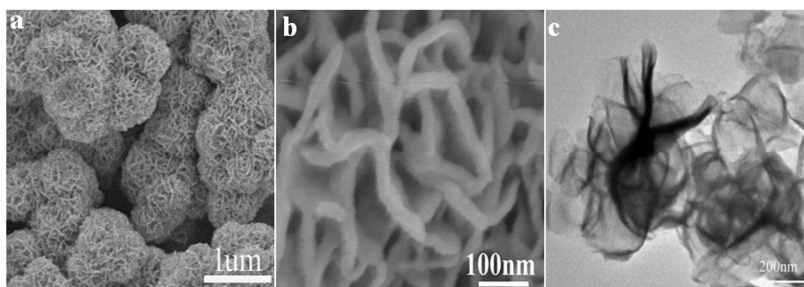


Figure 2. (a,b) SEM (c) TEM images of flower-like MoS₂.

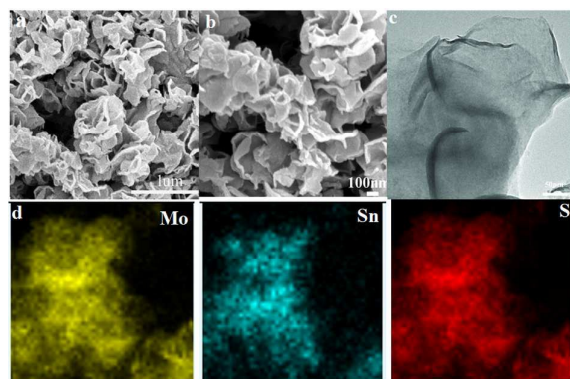


Figure 3. (a,b) SEM (c) TEM images of flower-like heterostructured SnS₂/MoS₂ (d) Corresponding elemental mapping of Mo, Sn, and S.

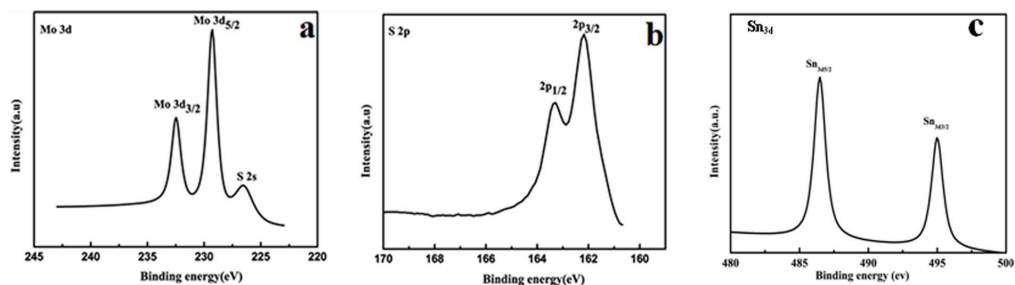


Fig. 4. XPS spectra of the flower-like heterostructured SnS₂/MoS₂. (a) high-resolution spectra for Mo 3d (b) high-resolution spectra for S 2p (c) high-resolution spectra for Sn 3d.

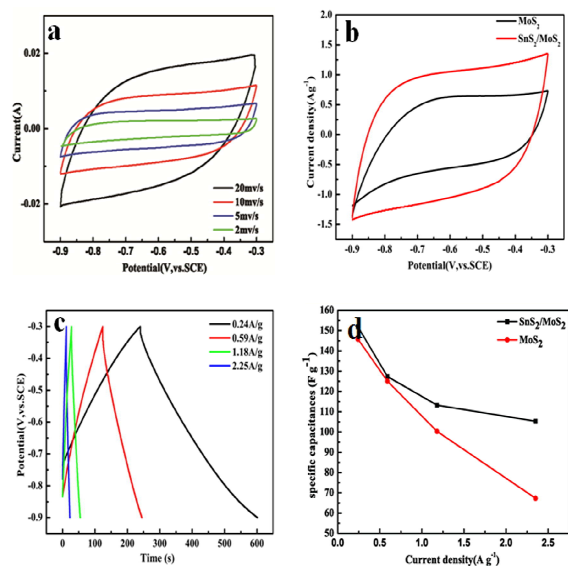


Figure 5. (a) CV curves of the SnS₂/MoS₂ electrodes at different scan rates (b) Normalized CV curves of the MoS₂ and SnS₂/MoS₂ electrodes at 10 mV s⁻¹ (c) Galvanostatic charge-discharge curves of SnS₂/MoS₂ electrodes at different current density. (d) Specific capacitances of MoS₂ and SnS₂/MoS₂ electrodes at different current density.

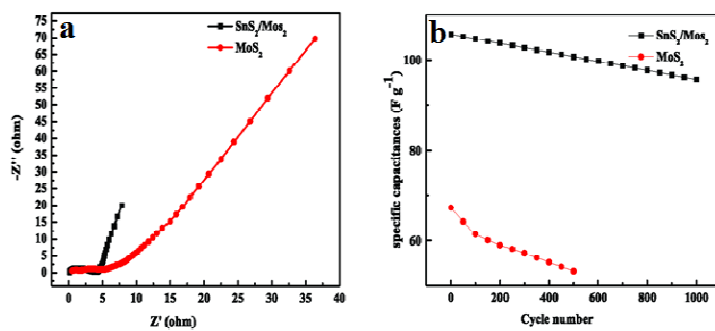
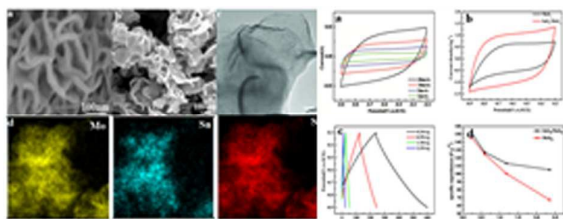


Figure 6.(a) Nyquist plots of MoS_2 and $\text{SnS}_2/\text{MoS}_2$ electrodes in 1 M KCl (b) Cycling stability of the MoS_2 and $\text{SnS}_2/\text{MoS}_2$ at a current density of 2.35 A g^{-1} .



3D heterostructured SnS₂/MoS₂ for enhanced Supercapacitor Behaviors was produced via One-Pot hydrothermal Synthesis